

Weak-interaction processes in stars: Applications to core-collapse supernovae

G. Martínez-Pinedo¹

*Institut d'Estudis Espacials de Catalunya, Edifici Nexus, Gran Capità 2,
E-08034 Barcelona, Spain*

*Institució Catalana de Recerca i Estudis Avançats, Lluís Companys 23,
E-08010 Barcelona, Spain*

Abstract

The role of weak-interaction processes in core collapse and neutrino nucleosynthesis is reviewed. Recent calculations of the electron capture rates for nuclei with mass numbers $A = 65$ – 112 show that, contrarily to previous assumptions, during core collapse electron capture is dominated by captures on heavy nuclei. Astrophysical simulations demonstrate that these rates have an important impact on the collapse. Neutrinos emitted by the collapsing core can interact with the overlying shells of the star producing substantial nuclear transmutations. This process known as ν -process seems to be responsible for the production of ^{138}La by charged current neutrino interactions with ^{138}Ba . The ν -process is then sensitive to the spectra of different neutrino species and to neutrino oscillations.

1 Introduction

Weak interaction processes play a very important role in the evolution of stars [1]. Stars with masses exceeding roughly $10 M_{\odot}$ reach a moment in their evolution when their iron core provides no further source of nuclear energy generation. At this time, they collapse and, if not too massive, bounce and explode in spectacular events known as type II or Ib/c supernovae. In the currently favored scenario [2], neutrinos deposit the energy of the explosion in the stellar medium which surrounds the nascent neutron star. This neutrino-driven wind is one of the most promising sites for the r-process nucleosynthesis [3] (see also the contributions of K.-L. Kratz and I. Borzov). Finally, in their way out of the star neutrinos interact with matter and contribute to the synthesis of several isotopes in what is known as the neutrino-process (ν -process).

¹The results presented in this talk have been obtained in collaboration with D. J. Dean, W. Haxton, A. Heger, W. R. Hix, H.-Th. Janka, E. Kolbe, K. Langanke, M. Liebendörfer, O. E. B. Messer, A. Mezzacappa, M. Rampp, J. Sampaio, S. E. Woosley

2 Electron capture rates in core collapse supernovae

The evolution of the star during collapse is determined by the competition between gravity, which forces the core to collapse, and the weak interaction that determines the rate at which electrons, that are the main contributors to the pressure, are captured. As the density of the star's center increases electrons become more degenerate and their chemical potential grows. For sufficiently high values of the chemical potential electrons are captured by nuclei producing neutrinos, which for densities $\lesssim 10^{11}$ g cm $^{-3}$, freely escape from the star, removing energy and entropy from the core. Thus entropy stays low during the collapse ensuring that nuclei dominate in the composition over free nucleons.

Before the collapse sets in, during the presupernova stage, i.e. at core densities $\lesssim 10^{10}$ g cm $^{-3}$, and proton-to-neutron ratios $Y_e \gtrsim 0.42$, nuclei with $A = 55$ – 65 dominate in the composition. The relevant rates for weak interaction processes were initially determined by Fuller, Fowler and Newman [4]. The rates have been recently improved based on modern data and state-of-the-art shell-model calculations [5]. Presupernova models utilizing these improved weak rates are presented in [6]. During collapse, temperatures and densities are high enough to ensure that nuclear statistical equilibrium is achieved. Then, for sufficiently low entropies, the matter composition is dominated by the nuclei with the largest binding energy for a given Y_e . In current collapse simulations a very simple description of electron capture on nuclei is used. The rates are estimated using an independent particle model (IPM) that assumes pure Gamow-Teller (GT) transitions [7]. In this model GT transitions are Pauli-blocked for nuclei with $N \geq 40$ and $Z \leq 40$ [8]. These nuclei dominate the composition for densities larger than a few 10^{10} g cm $^{-3}$. As a result, electron capture on nuclei ceases at these densities and the capture is entirely due to free protons. However, Pauli-blocking of the GT transitions is overcome once correlations [9] and temperature effects are taken in account [8, 10].

Correlations beyond the IPM produce a mixing of the pf shell with the levels of the sdg shell, in particular with the $g_{9/2}$ orbit. The description of the $B(E2, 0^+ \rightarrow 2_1^+)$ transition in the ^{68}Ni requires configurations where more than one neutron is promoted from the pf shell into the $g_{9/2}$ orbit [11] (see also O. Sorlin's contribution), unblocking the GT transitions for this $N = 40$ nucleus. Non-zero GT strengths have already been observed for ^{72}Ge [12] and ^{76}Se [13]. During core collapse electron capture occurs for temperatures $T \gtrsim 0.8$ MeV, which allow for thermal excitations from the pf shell to the sdg shell. The calculation of the electron capture rates then needs a model that is able to

describe the correlations and at the same time the high density of levels that can be thermally populated at moderate excitation energies. This model is the Shell Model Monte Carlo (SMMC) approach [14] which allows the calculation of nuclear properties at finite temperature in unprecedentedly large model spaces. To calculate electron capture rates for nuclei in the range $A = 65$ – 112 , we have carried out SMMC calculations in the full pf - sdg shells, using a residual pairing+quadrupole interaction. The SMMC calculations determine the average temperature-dependent occupation numbers of the various single particle orbitals, which then become the input in RPA calculations of the capture rate, where we consider allowed and forbidden transitions up to multipoles $L = 4$, including the momentum transfer dependence of the operators [15].

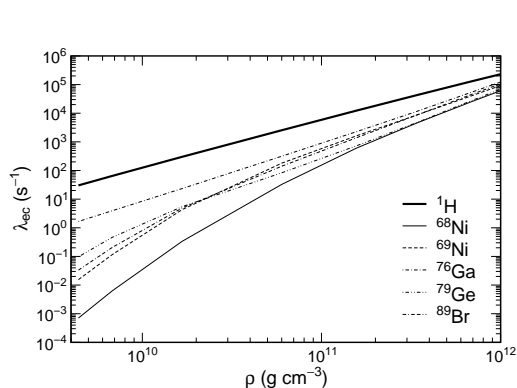


Figure 1: Comparison of the electron capture rates on free protons and selected nuclei as function of the electron chemical potential along a stellar collapse trajectory.

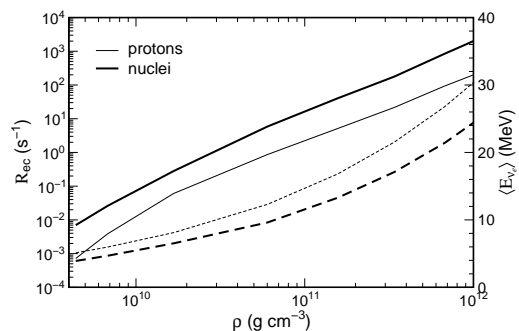


Figure 2: The reaction rates for electron capture on protons (thin line) and nuclei (thick line) are compared as a function of density along a stellar collapse trajectory. The dashed lines (right scale) show the related average energy of the neutrinos emitted by capture on nuclei and protons.

Figure 1 shows the electron capture rates for protons and selected nuclei along a stellar trajectory taken from [16]. For all nuclei the rates are dominated by GT transitions at low densities, while forbidden transitions contribute for $\rho \gtrsim 10^{11} \text{ g cm}^{-3}$. For the lowest densities the electron chemical potential ($\mu_e \approx 6 \text{ MeV}$ for $\rho = 5 \times 10^9 \text{ g cm}^{-3}$) is of the same order than the typical nuclear Q value. Then, the electron capture rates on nuclei are very sensitive to the Q -value and smaller than the rate on protons. For higher densities the chemical potential grows much faster than the Q -values, and the rates become basically independent of the heavy nucleus, depending only on the total strength. Due to the much smaller Q -value, the electron capture rate on free protons is larger than the rates on the abundant nuclei during collapse.

However, this is misleading as the low entropy keeps the protons significantly less abundant than heavy nuclei during the collapse. Figure 2 shows that the reaction rate for electron capture on nuclei ($R_h = \sum_i Y_i \lambda_i$, where the sum runs over all the nuclei present and Y_i denotes the number abundance of species i) dominates the one on protons ($R_p = Y_p \lambda_p$) by roughly an order of magnitude throughout the collapse, when the composition is considered. It should be noticed that figure 2 does not include the change in the collapse trajectory due to the inclusion of electron capture on nuclei. If considered, this produces a reduction of Y_e that reduces even more the abundance of free protons making the reaction rate on protons even smaller.

Electron capture on nuclei and on free protons differ quite noticeably in the neutrino spectra they generate. Figure 1 demonstrates that neutrinos from captures on nuclei have a mean energy 40–60% smaller than those produced by captures on protons. This is mainly due to the larger Q -value for capture on nuclei. Despite that, the total neutrino energy loss rate is larger when electron capture on nuclei is considered, caused by the increase in the total (nuclei plus protons) electron capture rate. The differences in neutrino spectra strongly influence neutrino-matter interactions, which scale with the square of the neutrino energy and are essential for collapse calculations [17]

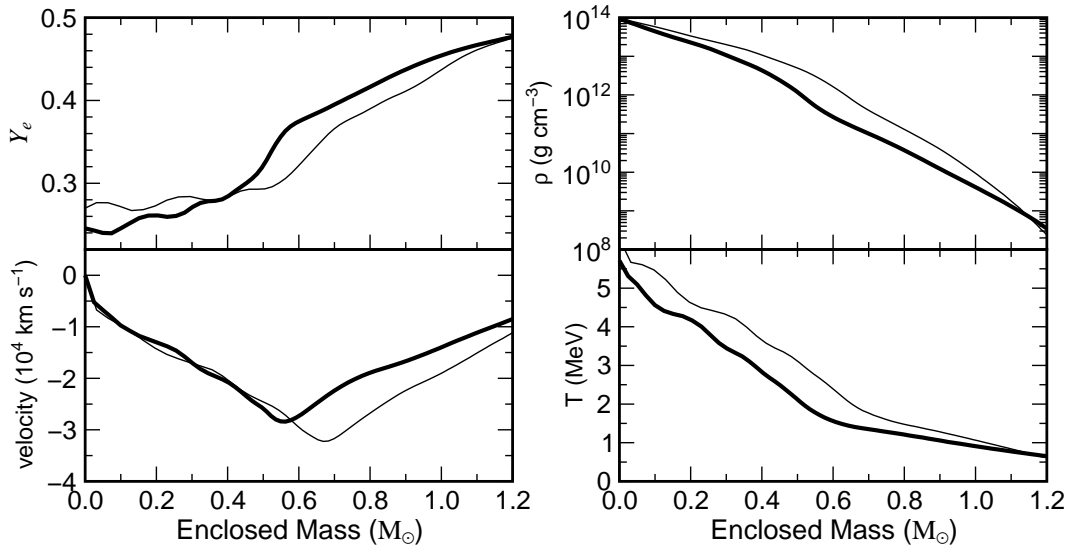


Figure 3: The electron fraction, velocity, density and temperature as functions of the enclosed mass at the moment when the center reaches nuclear matter densities for a $15 M_{\odot}$ star. The thin line is a simulation using the Bruenn parameterization [7] while the thick line is for a simulation using the combined LMP [5] and the present SMMC+RPA rate sets. Both models were calculated with Newtonian gravity.

Figure 3 shows the star profiles for several quantities obtained in collapse simulations carried out by the Oak Ridge collaboration [17] (similar results are obtained by the Garching collaboration) at the moment when the central density reaches $10^{14} \text{ g cm}^{-3}$. In the inner regions of the star, the additional electron capture on heavy nuclei results in more electron capture in the new models that produce a reduction in Y_e and a smaller central temperature. In outer regions, where nuclei $A < 65$ dominate, the new models predict less electron capture. This is so, because for these mass ranges the electron capture rates of ref. [5] are smaller than the ones used in the Bruenn parametrization [7]. Due to the smaller electron capture rates, these regions collapse more slowly so that the density and temperature are smaller in the new models. The velocity distribution shows a displacement in the minimum, which marks the eventual location of shock formation, by $0.1 M_\odot$.

3 Neutrino process

The total number of neutrinos (and antineutrinos) emitted by core collapse supernovae is about 10^{58} . Most of them are emitted during the cooling phase (lasting ~ 10 s) of the birth of a neutron star. When the flux of neutrinos passes through the overlying shells of heavy elements neutrinos can induce nuclear transformations despite the small neutrino-cross sections. In this way, only rare isotopes neighboring abundant nuclei can be produced. Of particular relevance for the ν -process are the neutral-current reactions induced by ν_μ, ν_τ and their antiparticles that have higher average energy than $\bar{\nu}_e$ and ν_e neutrinos (see ref. [18] for a recent review on neutrino spectra from core collapse supernovae). These neutrinos have enough energy to excite the GT and giant dipole resonances. They reside typically above particle thresholds and hence decay mainly by proton or neutron emission, generating new nuclides. The neutrino reaction rates are too small to affect the abundances of the parent nuclei, but they can noticeably contribute to the production of the much less abundant daughter nuclei.

Table 1 list some of the isotopes that can be produced by the ν -process and the most important reactions producing them. The most interesting neutrino nucleosynthesis occurs in the outer burning shells that have not been affected by the fatal collapse in the center. However, a little later the shock reaches these shells and the matter will be subjected to rather high temperatures initiating fast nuclear reactions involving also the nuclides just produced by the neutrino-induced reactions. Hence studies of the neutrino process depend on various neutrino-nucleus reaction rates and on the neutrino spectra and

Product	Parent	Reaction
^{11}B	^{12}C	$(\nu, \nu'n), (\nu, \nu'p)$
^{19}F	^{20}Ne	$(\nu, \nu'n), (\nu, \nu'p)$
^{138}La	^{138}Ba	(ν, e^-)
	^{139}La	$(\nu, \nu'n)$
^{180}Ta	^{180}Hf	(ν, e^-)
	^{181}Ta	$(\nu, \nu'n)$

Table 1: Main production reactions for the main products of the ν -process.

fluxes and they require a rather moderate nuclear network to simulate the effects of the re-processing by the shock. Moreover, in those regions where the ν -process is most effective, the neon-oxygen shell of the star, changes in the abundances due to the s-process during helium and carbon burning have to be accounted for. Investigations of the ν -process have shown that a few specific nuclei (^7Li , ^{11}B , ^{19}F) are made in significant amounts [19]. The production of ^{11}B is particularly relevant as the ν -process $^{11}\text{B}/^{10}\text{B}$ abundance ratio (~ 0.05) is significantly smaller than the solar ratio (0.25) [19]. Thus, there must be a second process which contributes to the production of both isotopes. These are reactions of energetic protons on ^{12}C in cosmic rays, which yield a ratio of about 0.5. As the ν -process is a primary process while cosmic ray spallation is a secondary process, the $^{11}\text{B}/^{10}\text{B}$ abundance ratio should have changed during the history of the galaxy [19].

Figure 4 shows the production factors (defined as the abundances in the ejected matter divided by the observed abundances) obtained in nucleosynthesis calculations for a $25 M_{\odot}$ star [20]. These simulations include the relevant neutrino cross sections and (γ, n) reactions (p-process) to study the production of ^{138}La and ^{180}Ta . Figure 5 shows that the nucleus ^{138}La is mainly made by the charged current interaction $^{138}\text{Ba}(\nu_e, e^-)^{138}\text{La}$, with a smaller contribution of the p-process reaction $^{139}\text{La}(\gamma, n)^{138}\text{La}$ (similar results were obtained in ref. [21]). ^{180}Ta is equally produced by the p-process reaction $^{181}\text{Ta}(\gamma, n)^{180}\text{Ta}$ and the ν -process reaction $^{180}\text{Hf}(\nu_e, e^-)^{180}\text{Ta}$ (see ref. [22] where the possibility of ^{180}Ta production in the s-process is discussed).

4 Conclusions

We have shown that the many neutron-rich nuclei that dominate the composition throughout the collapse of a massive star also dominate the rate of

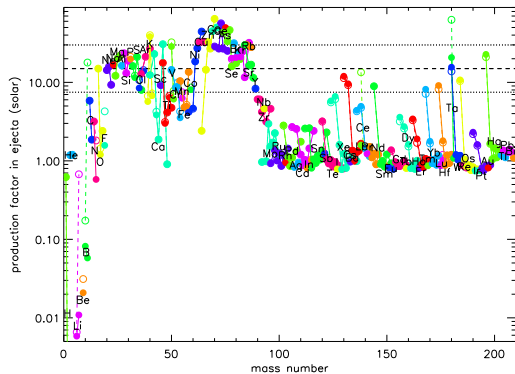


Figure 4: Production factors obtained in a $25 M_{\odot}$ star after explosion. The solid (open) symbols show the abundances obtained without (with) inclusion of neutrino reactions. Notice the huge increase in the abundance of ${}^7\text{Li}$, ${}^{11}\text{B}$, ${}^{19}\text{F}$, ${}^{138}\text{La}$ and ${}^{180}\text{Ta}$ (courtesy of A. Heger).

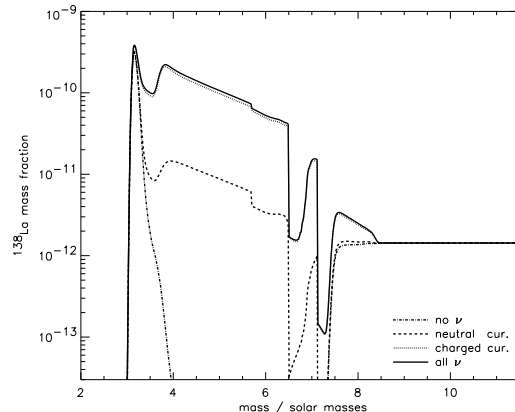


Figure 5: Contribution to the ${}^{138}\text{La}$ production as a function of mass coordinate in a $25 M_{\odot}$ star. The dash-dotted line gives the contribution without neutrino interactions (p-process only), the other lines show the p-process contribution plus different neutrino processes (courtesy of A. Heger).

electron capture. Astrophysics simulations demonstrate that these rates have a strong impact on the core collapse trajectory and the properties of the core at bounce. The evaluation of the rates has to rely on theory as a direct experimental determination of the rates for the relevant stellar conditions (i.e. rather high temperatures) is currently impossible. Nevertheless it is important to experimentally explore the configuration mixing between pf and sdg shell in extremely neutron-rich nuclei as such understanding will guide and severely constrain nuclear models. Such guidance is expected from future radioactive ion-beam facilities.

The ν -process is sensitive to the fluxes of ν_e and (ν_{μ}, ν_{τ}) that are expected to have different spectra and then can serve to test the different spectra predictions [18]. The ${}^{138}\text{La}$ nucleosynthesis is sensitive to neutrino oscillations, and would be significantly overproduced if supernova ν_{μ}, ν_{τ} neutrinos have a noticeably larger average energy and if they oscillate into ν_e neutrinos before reaching the ${}^{138}\text{La}$ production site in massive stars.

This work has been partly supported by the Spanish “Ministerio de Ciencia y Tecnología” under contract AYA2002-04094-C03-02

References

- [1] K. Langanke and G. Martínez-Pinedo, Rev. Mod. Phys. (2003), in press, nucl-th/0203071.
- [2] H.-T. Janka, K. Kifonidis, and M. Rampp, astro-ph/0103015.
- [3] T. A. Thompson, A. Burrows, and B. S. Meyer, Astrophys. J. **562** (2001) 887.
- [4] G. M. Fuller, W. A. Fowler, and M. J. Newman, Astrophys. J. Suppl. **42** (1980) 447; Astrophys. J. **252** (1982) 715; Astrophys. J. Suppl. **48** (1982) 279; Astrophys. J. **293** (1985) 1.
- [5] E. Caurier, K. Langanke, G. Martínez-Pinedo, and F. Nowacki, Nucl. Phys. A **653** (1999) 439; K. Langanke and G. Martínez-Pinedo, Nucl. Phys. A **673** (2000) 481; At. Data. Nucl. Data Tables **79** (2001) 1.
- [6] A. Heger, *et al.*, Phys. Rev. Lett. **86** (2001) 1678; Astrophys. J. **560** (2001) 307.
- [7] S. W. Bruenn, Astrophys. J. Suppl. **58** (1985) 771; A. Mezzacappa and S. W. Bruenn, Astrophys. J. **405** (1993) 637; **410** (1993) 740.
- [8] G. M. Fuller, Astrophys. J. **252** (1982) 741.
- [9] K. Langanke, E. Kolbe, and D. J. Dean, Phys. Rev. C **63** (2001) 032801.
- [10] J. Cooperstein and J. Wambach, Nucl. Phys. A **420** (1984) 591.
- [11] O. Sorlin, *et al.*, Phys. Rev. Lett. **88** (2002) 092501.
- [12] M. C. Vetterli, *et al.*, Phys. Rev. C **45** (1992) 997.
- [13] R. L. Helmer, *et al.*, Phys. Rev. C **55** (1997).
- [14] S. E. Koonin, D. J. Dean, and K. Langanke, Phys. Repts. **278** (1997) 2.
- [15] K. Langanke, *et al.* submitted to Phys. Rev. Lett., astro-ph/0302459.
- [16] A. Mezzacappa, *et al.*, Phys. Rev. Lett. **86** (2001) 1935.
- [17] W. R. Hix *et al.* in preparation.
- [18] M. T. Keil, G. G. Rafelt, and H.-T. Janka (2002), astro-ph/0208035.
- [19] S. E. Woosley and T. A. Weaver, Astrophys. J. Suppl. **101** (1995) 181; S. E. Woosley, *et al.*, Astrophys. J. **356** (1990) 272.
- [20] A. Heger, *et al.*, in preparation.
- [21] S. Goriely, M. Arnould, I. Borzov, and M. Rayet, Astron. & Astrophys. **375** (2001) L35.
- [22] D. Belic, *et al.*, Phys. Rev. C **65** (2002) 035801.